**Nucleation and Initial Stages of Growth During the Atomic Layer Deposition** 

(ALD) of Titanium Oxide on Mesoporous Silica

Wang Ke, <sup>1</sup> Yang Liu, <sup>2</sup> Xuelong Wang, <sup>3</sup> Xiangdong Qin, <sup>1,‡</sup> Limei Chen, <sup>1</sup> Robert Palomino, <sup>3</sup> Juan

Pablo Simonovis, <sup>1</sup> Ilkeun Lee, <sup>1</sup> José Rodriguez, <sup>3</sup> Anatoly I. Frenkel, <sup>2,3</sup> Ping Liu, <sup>3</sup> Francisco

Zaera,1,\*

Department of Chemistry, University of California, Riverside, CA 92521, USA

2 Department of Materials Science and Chemical Engineering, Stony Brook University, Stony

Brook, NY 11794, USA

3 Chemistry Division, Brookhaven National Laboratory, Upton, NY 11973, USA

\* Corresponding author: zaera@ucr.edu

Abstract

The ability to deposit thin films on solid surfaces by chemical means is highly desirable, but

chemical depositions are prone to affect the final properties of the film. To better understand the

origin of these complications, the initial stages of the atomic layer deposition (ALD) of titania

films on silica mesoporous materials were characterized. Adsorption-desorption isothermal

measurements indicated that the films grow uniformly throughout the length of the pores, in a

layer-by-layer fashion, as desired. However, the initial films proved to have surprisingly low

densities, below 1 g/ml, more than 4 times lower than that of bulk titania. XRD, Visible/UV and

‡ Present Address: ASM America, Phoenix, AZ 85034, USA

X-ray absorption spectroscopy data, together with electron microscopy, pointed to the amorphous nature of the first few monolayers, and EXAFS and <sup>29</sup>Si CP/MAS-NMR results to an initial growth via the formation of individual tetrahedral Ti-oxide units on isolated Si–OH surface groups. DFT calculations were used to propose a model where the initial growth occurs laterally, away from the nucleation centers, to create an open 2D tetrahedral-Ti-oxide network.

### Main

Many applications require the deposition of thin films on solid materials. This is often carried out by physical means (evaporation, sputtering), but on solids with complex structures, in particular in porous materials, it is better accomplished by using chemical reactions; the isotropic nature of the reactions of gases with surfaces affords an even deposition across the entire surface regardless of topography. Atomic layer deposition (ALD), a chemical approach where the overall depositing reaction is split into two or more complementary and self-limiting steps, has received particular attention recently because of its ability to offer film growth with sub-monolayer control.<sup>1, 2, 3</sup> However, chemical film deposition processes bring about additional complexity. For one, in the initial ALD cycles, the depositing chemicals must interact and react with specific sites on the original substrate, on so-called nucleation sites; in oxides such as silica or alumina, these typically are isolated hydroxo groups.<sup>1, 4</sup> The catch is that the density of such sites on the surface is often low (there are about 2 silanol, Si–OH, groups per square nanometer on most silica surfaces).<sup>5</sup> That can limit the deposition rate, and, more importantly, affect the properties of the new material. In this study, we have characterized the initial growth of titania films on a silica mesoporous material,

SBA-15, to better understand its mechanism at a molecular level. One particularly interesting observation deriving from this work is the fact that, although the films do grow uniformly over the entire surfaces of the inside of the pores of SBA-15, their density is particularly low, initially a factor of approximately 4 lower than that of crystalline titania. A combination of characterization techniques was complemented with quantum mechanics calculations to explain this behavior. A model was developed where initial hydroxo-terminated titanium monomers form on the silica nucleation centers, and where the growth of the first layer of the titania film progresses laterally away from those centers, creating a 2D network of titanium oxide tetrahedral units. The resulting film is therefore amorphous and displays an open structure. Subsequent layers can then grow on top, at higher densities that rapidly approach bulk values (within 3 - 4 monolayers). This initial film growth mechanism is likely to be general. The unique properties of the substrate-growing film interface obtained via ALD may affect their use in many applications, especially in microelectronics fabrication, but can also be quite beneficial in other areas such as catalysis, where the amorphous nature of the films may facilitate redox reactions.

SBA-15 was chosen as the substrate for these studies in order to take advantage of its simple and well-defined mesoporous structure, which consists of one-dimensional long pores approximately 6 – 7 nm in diameter.<sup>6</sup> Because of the narrow distribution of the pore size in SBA-15, adsorption-desorption isotherm measurements can be used to assess the uniformity of films deposited by ALD on this material, and also to measure the rate of film growth.<sup>7,8</sup> This approach is illustrated by the data provided in Figure 1, which correspond to the ALD of titania films on SBA-15 using tetrakis(dimethylamido)titanium(IV) (TDMAT) and water. Figure 1a shows the pore size distributions measured for samples obtained after different numbers of TiO<sub>2</sub> ALD cycles (from 0

to 10), whereas Figure 1b reports the results for the evolution of the average pore size (<d>), total surface area (A), and total pore volume (V). As expected, the pore diameter decreases with increasing number of ALD cycles, as the pores are closed up by the growing new TiO<sub>2</sub> film. The growth rate is approximately constant, estimated from the plot of <d> vs. ALD cycle number at R = 1.15  $\pm$  0.05 Å/cycle. Critically, the pores retain the narrow size distribution initially seen in pristine SBA-15, a fact that points to the uniform nature of the films being deposited and to the layer-by-layer growth mechanism attained in this ALD process. The linear and square dependences of A and V versus <d>, respectively, provide additional confirmation of this behavior (Supplementary Figure S1).

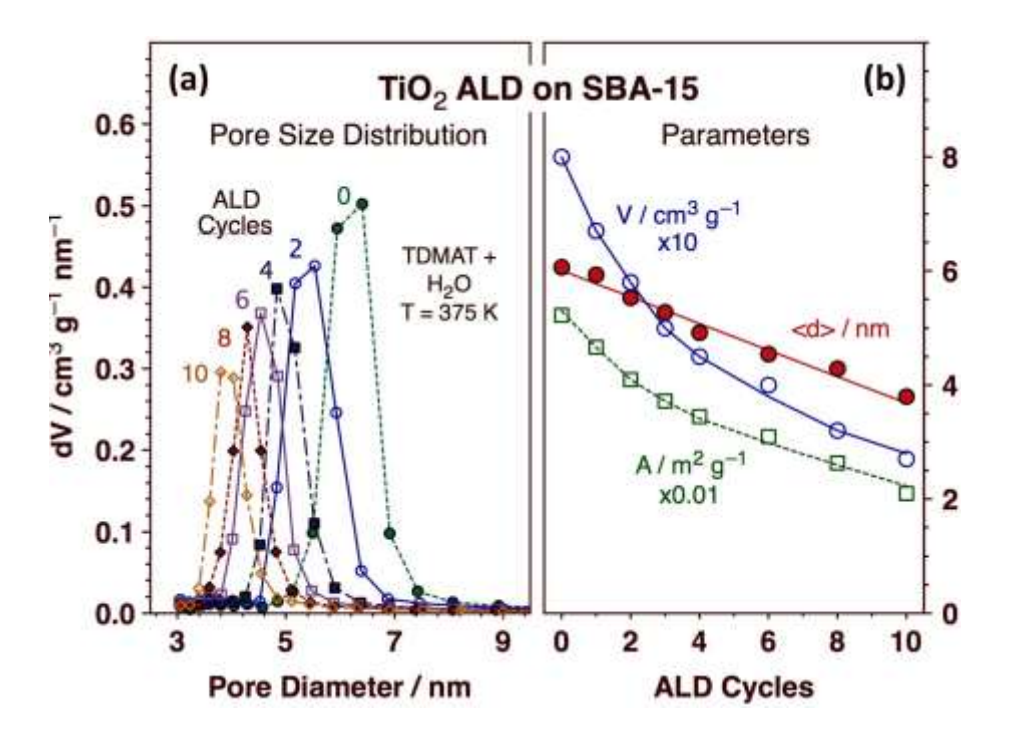


Figure 1. Pore size distributions (a) and average pore diameter, area, and volume (b) of SBA-15 samples on which TiO<sub>2</sub> films have been deposited as a function of the number of TiO<sub>2</sub> ALD cycles used.

The mass of the TiO<sub>2</sub> added to the SBA-15 substrate during the ALD film growth process can be

estimated by using a number of techniques. The amount of TiO<sub>2</sub> deposited after the first cycle was independently determined by three methods: by directly measuring the gain in weight of the solid using a microbalance, by energy dispersive X-ray analysis (EDX) during electron microscopy imaging, and by inductively coupled plasma atomic emission spectroscopy (ICP-AES); all three measurements agreed within experimental error, and yielded a value of about 0.80 mmol TiO<sub>2</sub>/g SBA-15 (Supplementary Information Figure S2). The mass uptake was then followed as a function of the number of TiO<sub>2</sub> ALD cycles using ICP-AES (Figure 2a, blue open squares). The uptake displays an approximately linear behavior with ALD cycle number.

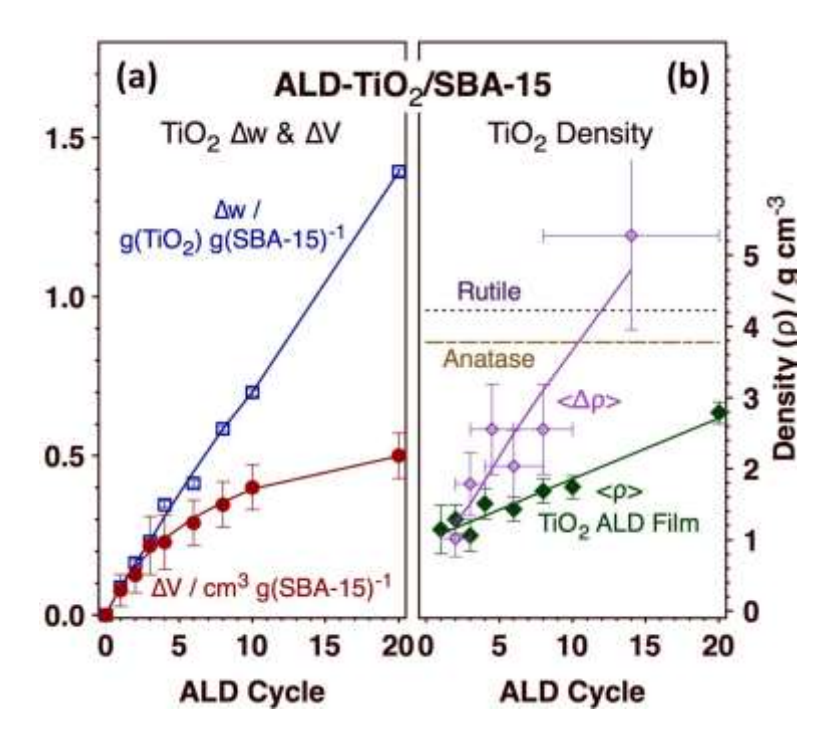


Figure 2. (a) Evolution of the mass and volume of the TiO<sub>2</sub> films as a function of the number of ALD cycles used. (b) Film density estimated from the data in Panel (a), both in cumulative (solid green circles) and differential (open purple diamonds) forms.

The mass uptake data were combined with the volume of the films, estimated from the information in Figure 1b (Figure 2a, red filled circles) to estimate the density of these titania films. The results,

shown in Figure 2b, are surprisingly low. The data are presented both in cumulative (Figure 2b, filled green diamonds) and differential (Figure 2b open purple diamonds) forms to better highlight the evolution of this density versus the number of TiO<sub>2</sub> ALD cycles, that is, versus film thickness. To notice is the exceptionally low value determined for the films grown after the first 1 – 4 cycles, approximately 1 g/cm<sup>3</sup>; this is to be compared with reported values of 3.78 and 4.23 g/cm<sup>3</sup> for the anatase and rutile crystalline forms of titania, respectively. Densities this low are only seen with oxides prepared via xerogel or sol-gel synthesis, and are virtually unknown for TiO<sub>2</sub>.<sup>9, 10, 11</sup> The TiO<sub>2</sub> film density does increase with increasing film thickness, and approaches bulk-like values after 10 – 15 TiO<sub>2</sub> ALD cycles.

Further confirmation of the initial low density of the  $TiO_2$  films grown by ALD was obtained from X-ray photoelectron spectroscopy (XPS) data. The O 1s XPS signal displays two clearly separate features at 532.8 and 530.6 eV binding energies (BEs; Supplementary Information Figure S3a)), which can be easily ascribed to  $SiO_2$  and  $TiO_2$ , respectively. It was found that the total area of the O 1s XPS trace goes down with increase  $TiO_2$  film thickness, from which its was estimated that the density of oxygen atoms in that film is approximately 2/3 of that of the underlying silica substrate (Supplementary Information Figure S3b). The film deposition rate was estimated from the O 1s XPS, Ti 2p XPS, and Ti  $L_{2,3}$  X-ray absorption near-edge structure spectroscopy (XANES, also know as NEXAFS) signals to be  $0.95 \pm 0.20$  Å/cycle, in reasonable agreement with the value obtained using the adsorption-desorption isotherms (Figure 1).

The film thicknesses was calibrated in terms of monolayers to better understand the low film density observed in the initial stages of deposition. Several approaches were followed to this end.

First, the mass uptake behavior can be normalized to the initial number of nucleation sites (surface Si–OH groups) on SBA-15, which has been reported to be 1.8 mmol/g.<sup>5</sup> On that basis, the data in Figures 2 and S2 indicate that it should take somewhere between 2 and 3 TiO<sub>2</sub> ALD cycles to react all of those nucleation sites. A more direct way to follow this process is by estimating the surface coverage of the silanol groups via the quantification of the peak due to the corresponding O–H stretching vibrational mode in the infrared absorption spectra (IR) of the solids. The results from those studies are presented in Figure 3a. There, an initial peak at 3752 cm<sup>-1</sup> associated with the SBA-15 silanol surface groups is seen to decrease in intensity and to be replaced by a new feature at 3748 cm<sup>-1</sup> due to hydroxo surface groups on the new titania film as the deposition proceeds. The transition appears to be complete after 3 – 4 ALD cycles. Alternatively, the surface Si and Ti atoms can be titrated by adsorption of carbon monoxide at low (125 K) temperatures (Figure 3b). In that case, the C–O stretching frequency transitions from 2155 cm<sup>-1</sup> (from adsorption on silica) to 2190 cm<sup>-1</sup> (on titania) after approximately 3 ALD cycles. Combining all these data, it is concluded that the first monolayer saturates after 3 ± 1 TiO<sub>2</sub> ALD cycles.

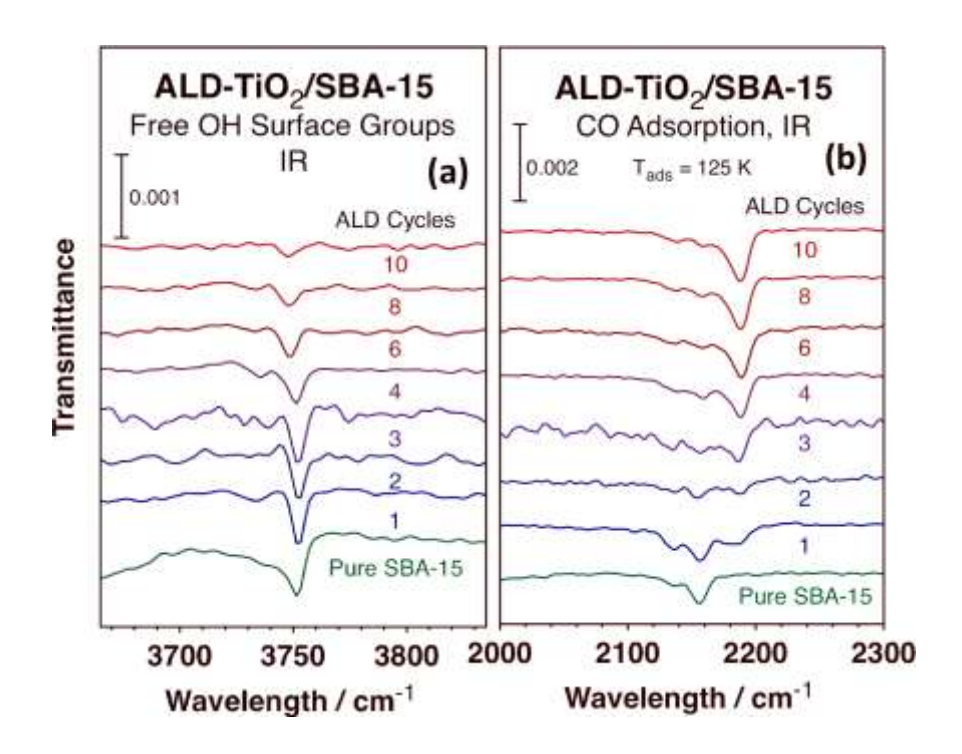


Figure 3. IR spectra in the O–H stretching (a) and C–O stretching (after adsorption of CO) regions for SBA-15 solids treated with various number of TiO<sub>2</sub> ALD cycles.

The next step to understand the molecular details of the growth of  $TiO_2$  films on SBA-15 by ALD was to evaluate their degree of crystallinity. To help with this assessment, X-ray diffraction (XRD) data (Supplementary Information Figure S4a) and transmission electron microscopy (TEM) images (Supplementary Information Figures S4b to S4e) were acquired for the sample obtained after  $10 \text{ Ti}O_2$  ALD cycles as a function of annealing temperature. The titania films were found to be amorphous unless calcined at high temperatures ( $T \ge 1075 \text{ K}$ ), at which point the titania appears to migrate to the mouth of the pores and to form small titania crystallites. Comparison of the Ti K-edge XANES spectra of samples obtained after various numbers (2, 3, 4, and 10) of  $TiO_2$  ALD cycles with those of crystalline (anatase, rutile, brookite) titania confirms that conclusion (Supplementary Information Figure S5). It was also found, using visible/UV absorption

spectroscopy, that the amorphous thin films made by ALD display bandgaps larger than those corresponding to crystalline titania (Supplementary Information Figure S6).<sup>13, 14</sup> The bandgap is reduced as the films become thicker, asymptotically approaching the bulk value.

The details of the coordination to the silica surfaces of the  $TiO_x(OH)_y$  units formed in the initial stages of the  $TiO_2$  ALD process were probed by using  $^{29}Si$  cross-polarization magic-angle spinning nuclear magnetic resonance (CP/MAS NMR). <sup>15, 16, 17</sup> The results from those studies, displayed in Figure 4, indicate that reactivity during the  $TiO_2$  ALD process occurs preferentially at isolated silanol groups: note the selective suppression of the signal intensity of the  $Q_3$  peak at -102 ppm ascribed to those species after 4  $TiO_2$  ALD.

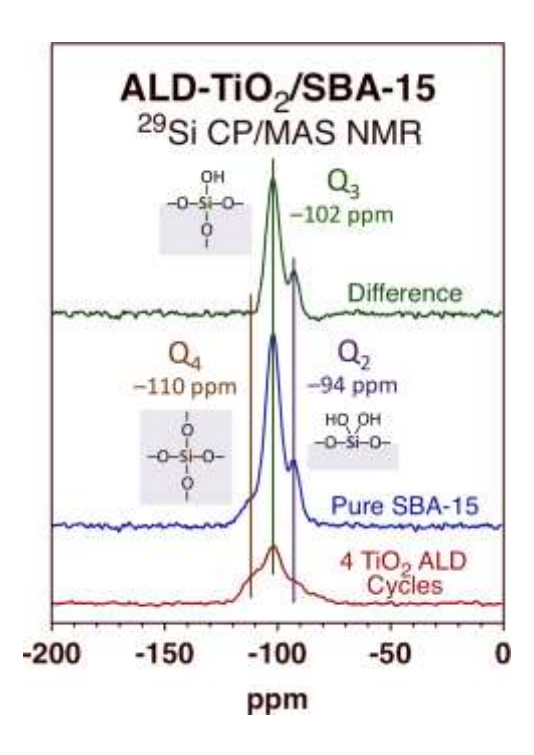


Figure 4. <sup>29</sup>Si CP/MAS NMR spectra for SBA-15 before and after 4 TiO<sub>2</sub> ALD cycles. The green trace, which corresponds to the difference between the two, indicates preferential nucleation at isolated OH surface groups.

Complementary information on the structural details of the titania sub-units that form on those isolated silanol nucleation centers was extracted from the extended X-ray absorption fine structure (EXAFS) data provided in Supplementary Information Figure S7. The results from fitting of the radial distribution data by allowing all coordination numbers, average Ti-O bond distances and Debye Waller factors to be optimized are reported in Supplementary Information Table S1. They indicate low coordination numbers (CN) for all TiO<sub>2</sub> films obtained via ALD, CN ~ 3. A refined set of data obtained by fixing these CNs at a more chemically meaningful value of 4 is provided in Table 1. The observations to highlight here are that the initial TiO<sub>x</sub>(OH)<sub>v</sub> sub-units formed on the silica surface appear to have tetrahedral, not octahedral, structures, yet the bond lengths are longer than those seen for other tetrahedral titania and more akin to what is seen in octahedral coordinations. 18, 19 In fact, the Ti-O bond length estimated here for the 10 TiO2 ALD/SBA-15 sample is quite close to that seen in (octahedral coordination) anatase. We are not aware of any other examples of tetrahedral coordination in titania with such bond lengths. This combination of low coordination numbers and long Ti-O bond distances contributes to the low density of the resulting titania films. 9, 20, 21, 22, 23, 24 Additional analysis of the EXAFS data to extract information about the second coordination sphere proved unreliable, but did point to low (1 to 2) Ti-O-Si or Ti-O-Ti coordination numbers (Supplementary Information Tables S2 and S3), consistent with the isolated nature of the initial titania sub-units as they grow out of the silica nucleation centers.

Table 1. Average Ti–O bond distances and Debye Waller factors estimated from EXAFS data for SBA-15 samples after TiO<sub>2</sub> deposition using 3, 4, and 10 ALD cycles. The coordination number of O atoms around the Ti centers was fixed at a value of 4 for these calculations.

Sample	<d(ti-o)> / Å</d(ti-o)>	$\sigma^2(Ti-O) / \mathring{A}^2$

3 TiO <sub>2</sub> ALD Cycles/SBA-15	$1.851 \pm 0.045$	$0.0067 \pm 0.0030$
4 TiO <sub>2</sub> ALD Cycles/SBA-15	$1.866 \pm 0.039$	$0.0062 \pm 0.0026$
10 TiO <sub>2</sub> ALD Cycles/SBA-15	$1.931 \pm 0.045$	$0.0102 \pm 0.0018$

Finally, density functional theory (DFT) calculations were carried out to help develop a model for the chemistry involved in the early stages of the TiO<sub>2</sub> ALD process consistent with the experimental data and observations described above. According to the previous studies (Ref?), the silica substrate was emulated by using two different facets ((001) and (110)) of β-cristobalite, partially derivatized with vincinal and solixane silica subunits to cap some of the terminal silanol surface groups in order to obtain an initial OH surface coverage,  $\theta_{OH,init} = 1.97 \text{ OH/nm}^2 = 2.14$ mmol/g, close to that observed experimentally for SBA-15 (Supplementary Information Figure S8). The titania ALD process was then simulated by adding individual TiO<sub>x</sub>(OH)<sub>y</sub> units to the Si– OH nucleation sites, one per β-cristobalite unit cell at a time, to sequentially form individual Si-O-Ti(OH)<sub>3</sub> surface units (which we denote as monomers), dimers, tetramers, rows, and monolayer networks, respectively (Figure 5). The first thing that was learned from these calculations is that the titania units that are deposited on the silica surfaces are much more stable in tetrahedral than octahedral form: any Si-O-Ti(OH)<sub>5</sub> units that may form on the surface is thermodynamically driven to decompose into  $Si-O-Ti((OH)_3 + H_2O + 1/2 O_2$  (Supplementary Information Figure S9). Also, in all cases the individual titania units prefer mono- to bi-coordination to the silica surface.

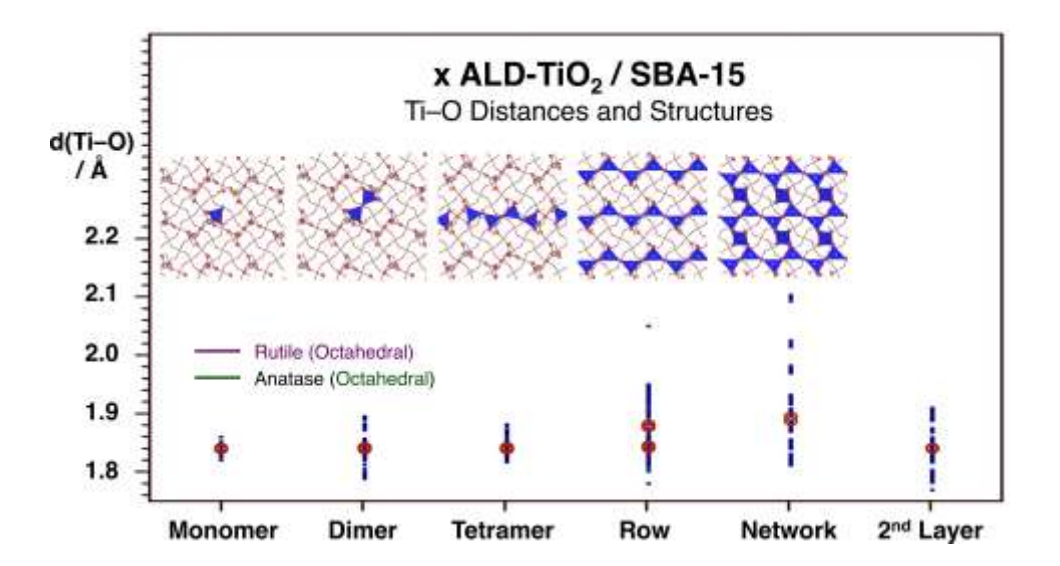


Figure 5. DFT calculations of the structures and Ti–O bond lengths of  $TiO_x(OH)_y$  units deposited on  $\beta$ -cristobalite as a function of coverage. The structures correspond to the (001)  $\beta$ -cristobalite surface, but similar results were obtained with the (110) facet. The blue dots correspond to individual bond lengths determined within the several stable configurations obtained in the DFT calculations, whereas the red circles are averages over all the bond distances within each configuration. The average Ti–O bond distances for octahedral anatase and rutile are also provided for reference.

In addition, the Ti–O bond distances calculated by DFT (Figure 5) are longer than expected, and in good agreement with the values estimated from the EXAFS experiments (Table 1). For instance, the average bond lengths calculated for the  $TiO_x(OH)_y$  rows is  $<d(Ti-O)>=1.86\pm0.02$  Å, close to the values obtained experimentally after 3 - 4 ALD cycles,  $<d(Ti-O)>=1.86\pm0.04$  Å; these both correspond to a surface density of approximately 2 Ti atoms per nm². Moreover, the Ti–O bond lengths increase with increasing Ti surface coverage, as seen experimentally and corroborated by the DFT calculations. For example, after 10  $TiO_2$  ALD cycles,  $<d(Ti-O)>_{EXAFS}$  = 1.93  $\pm$  0.04 Å (Table 1), and for the monolayer network  $<d(Ti-O)>_{DFT}$  = 1.89  $\pm$  0.01 Å. The combination of the titania surface units having tetrahedral structures with long Ti–O bonds more

typical of octahedral configurations and the fact that those bond lengths increase with increasing surface coverage within the first monolayer are all unique properties with no precedent in the literature that we are aware of. More details on the structures and energetics of these calculated titania layers are provided in Supplementary Information Figure S10. Finally, the DFT calculations also reproduce qualitatively the trends in bandgap energies seen in Supplementary Information Figure S6 (Supplementary Information Figures S11 and S12).

In summary, we have shown that the growth of titania films on mesoporous silica can be controlled at a submonolayer level by ALD. The growing films cover the inside surface of the pores evenly in spite of the high aspect ratio of those structures, but they initially display very low densities, less that one quarter of those seen in crystalline titania. In addition, it was determined that the initial nucleation reaction, which occurs on isolated silanol groups on the silica surface, produces tetrahedral (not octahedral, as seen in bulk titania) Si–O–Ti(OH)<sub>3</sub> units with unusually long Ti–O bond distances. The film then grows out of those nucleation sites to eventually form a network of TiO<sub>x</sub>(OH)<sub>y</sub> units with an open structure. The film density increases monotonically with coverage, and approaches bulk values after the buildup of approximately 3 - 4 layers. We have used the titania-SBA-15 system as a prototype, but believe that the conclusions reached here about the unique properties of the first few layers of oxide films grown by chemical means may be quite general and apply to other ALD processes on porous materials.

### Methods

The titania films were deposited on commercial SBA-15 (ACS Material) using a homemade ALD reactor described in detail elsewhere,<sup>8</sup> alternating exposures to TDMAT (tetrakis(dimethylamido)Ti(IV), Aldrich-Sigma, 99.999% purity in a trace metals basis) and deionized water. Typical cycle times were TDMAT: $N_2$ : $H_2O:N_2 = 20$  min:50 min:2 min:50 min, and the depositions were normally carried out at 375 K, the same for both the sample and the reactor; the precursor was kept at 315 K.

Adsorption–desorption isotherm measurements were carried out in a NOVA@2000e gas sorption system, using N<sub>2</sub> as the adsorbent. Data analysis was carried out by using the Nova Win software: pore distributions and total pore volumes were estimated using the BJH (Barrett–Joyner–Halenda) equations for Type IV isotherms, whereas total surface areas were calculated by using the BET (Brunauer–Emmett–Teller) isotherm.

Transmission Fourier transform infrared (FTIR) spectroscopy characterization experiments were performed on a Bruker Tensor 27 FTIR spectrometer equipped with a deuterated triglycine sulfate (DTGS) detector. About 15 mg of the catalyst was pressed into a self-supporting wafer and loaded inside a homemade quartz cell with NaCl windows.<sup>25</sup> The cell was evacuated and cooled down to 123 K (using liquid nitrogen), and IR spectra of the bare samples were acquired. Afterward, they were exposed to 50 Torr of CO (Matheson Tri-Gas, ≥99.5% purity) for 0.5 h, and the cell was evacuated for 10 min. IR spectra were recorded from 125 to 475 K at 20 K intervals as the sample and cell were warmed up (data not shown), and corrected using background spectra obtained under the same condition before adsorption.

Titanium loadings were quantified by inductively coupled plasma atomic emission spectrometry (ICP-AES), using a PerkinElmer Optima 7300DV ICP-OES apparatus that combines an SCD detector and an echelle optical system which enables the unit to measure all wavelengths simultaneously, in the ultraviolet wavelength range from 165 to 403 nm and in the visible wavelength range from 404 to 782 nm.

Scanning transmission electron microscopy (STEM) images were obtained using a FEI Titan Themis 300 instrument equipped with a X-ray spectrometer for energy dispersion spectroscopy (EDX) imaging. The crystallinity of the samples was evaluated by X-ray diffraction (XRD), using a Bruker D8 Advance Diffractometer with Cu K $\alpha$  radiation ( $\lambda$  = 1.5406 Å). The bandgap values were extracted from visible/UV diffuse reflectance spectra taken using a Varian Cary 500 double beam scanning UV/Vis/NIR spectrophotometer.

XPS data were collected with a commercially available AP-XPS system (SPECS Surface Nano Analysis GmbH, Germany) using a Mg K<sub>α</sub> anode (1253.6 eV). Ti L<sub>2,3</sub>-edge NEXAFS data were collected at the IOS beam line (23ID-2) of the NSLS-II facility of Brookhaven National Laboratory, following the total electron yield (TEY) by measuring the drain current. The photon flux was  $10^{13}$  photons/s, and monocrystal gratings with 150, 400 and 1200 lines/mm were employed. The resolution was  $E/\Delta E = 104$ , and the spot size (unfocused beam) ~50 μm (vertical) x ~150 μm (horizontal). Ti K-edge XAS data were acquired at the NSLS II BL 7-BM beamline, in fluorescence mode using a PIPS detector. The data from a minimum of 30 scans (each scan was about 45 seconds long) were averaged to obtained each spectrum.

Solid-state <sup>29</sup>Si CP/MAS-NMR spectra were acquired on a Bruker Avance 600 spectrometer, employing a cross-polarization contact time of 2 ms, a <sup>1</sup>H decoupling bandwidth of 80 kHz, and a recycle time of 3 s. Data were acquired as 12,000 co-added 2,048 complex data point FIDs with a 100 kHz sweep width. Post acquisition processing consisted of exponential multiplication with 200 Hz of line broadening and zero filling to 4,096 data points. Chemical shifts were referenced to an external DSS sample.

DFT calculations were performed with the Vienna Ab Initio Simulation Package (VASP),[ref] using the projection-augmented wave (PAW) approach.[ref] The generalized gradient approximation (GGA) type exchange-correlation functional[ref] in the parametrization of Perdew, Burke, and Ernzerhof (PBE) was adopted.[ref] The energy cutoff for the basis set of wave functions was set to 500 eV. The k-mesh was generated at least denser than the density of one point per 0.05 Å<sup>-3</sup> with the Monkhorst-Pack method.[ref] For the relaxation of the model structures, the forces felt by each atom were well converged to a level smaller than 0.05 eV/Å. For the DOS and bandgap calculations, the GGA+U method was used to address the strong correlation between the 3d orbital electrons of Ti with an effective U value of 4.2 eV.[ref]

## Acknowledgements

Financial support for this project was provided by a grant from the U.S. Department of Energy (DOE), Office of Science, Basic Energy Sciences, Materials Sciences and Engineering (MSE) Division, under Award No. DE-SC0001839. AIF acknowledges support from the National Science Foundation Grant number DMR-1911592 for the XAS measurements and data analysis. The Ti K-edge XAS and Ti L2,3-edge NEXAFS data were acquired at beamlines 7-BM (QAS) and 23-ID-2 (IOS), respectively, of the National Synchrotron Light Source II (NSLS-II), a U.S.

DOE Office of Science User Facility operated for the DOE Office of Science by Brookhaven National Laboratory (BNL) under Contract No. DE-SC0012704. QAS beamline operations were supported in part by the Synchrotron Catalysis Consortium (U.S. DOE, Office of Basic Energy Sciences, Grant No. DE-SC0012335). The DFT calculations were performed using computational resources at the Center for Functional Nanomaterials, which is a U.S. DOE Office of Science Facility, and the Scientific Data and Computing Center, a component of the Computational Science Initiative, at BNL. The XPS and DFT the research carried out at BNL was supported by the U.S. Department of Energy, Office of Science and Office of Basic Energy Sciences under contract No. DE-SC0012704. JPS is supported through the NSLS-II Director's Postdoctoral Program jointly with the BNL Chemistry Division.

#### **Author Contributions**

- Wang Ke: Performed the ALD film growth and the adsorption, ICP-AES, IR, NMR, and XRD experiments.
- Yang Liu: Performed the Ti K-edge XAS experiments.
- Xuelong Wang: Performed and analyzed the DFT calculations.
- Xiangdong Qin: Supervised the preparation and initial characterization of the samples.
- Limei Chen: Performed the Visible/UV absorption characterization experiments
- Robert Palomino: Performed the XPS and Ti L<sub>2,3</sub>-egde XAS experiments.
- Juan Pablo Simonovis: Analyzed the XPS and Ti L<sub>2,3</sub>-egde XAS data.
- Ilkeun Lee: Performed the microscopy imaging and EDX experiments.
- José Rodriguez: Supervised the XPS and Ti L<sub>2,3</sub>-egde XAS experiments.
- Anatoly I. Frenkel: Supervised the Ti K-edge XAS experiments and analyzed the data.
- Ping Liu: Supervised the DFT calculations.
- Francisco Zaera: Principal investigator, conceived the study, coordinated and supervised all work, analyzed the data, and wrote the manuscript.

# **Competing Interests**

The authors declare no competing financial interests.

#### References

- 1. George SM. Atomic layer deposition: An overview. *Chem Rev* 2010, **110**(1): 111-131.
- 2. Leskelä M, Niinistö J, Ritala M. 4.05 Atomic Layer Deposition. In: Hashmi S, Batalha GF, Van Tyne CJ, Yilbas B (eds). *Comprehensive Materials Processing*, vol. 4. Elsevier: Oxford, 2014, pp 101-123.
- 3. Richey NE, de Paula C, Bent SF. Understanding chemical and physical mechanisms in atomic layer deposition. *J Chem Phys* 2020, **152**(4): 040902.
- 4. Lu J, Elam JW, Stair PC. Atomic layer deposition—Sequential self-limiting surface reactions for advanced catalyst "bottom-up" synthesis. *Surf Sci Rep* 2016, **71**(2): 410-472.
- 5. Ide M, El-Roz M, De Canck E, Vicente A, Planckaert T, Bogaerts T, *et al.* Quantification of silanol sites for the most common mesoporous ordered silicas and organosilicas: total versus accessible silanols. *Phys Chem Chem Phys* 2013, **15**(2): 642-650.
- 6. Zhao D, Feng J, Huo Q, Melosh N, Fredrickson GH, Chmelka BF, *et al.* Triblock Copolymer Syntheses of Mesoporous Silica with Periodic 50 to 300 Angstrom Pores. *Science* 1998, **279**(5350): 548-552.
- 7. Mahurin S, Bao L, Yan W, Liang C, Dai S. Atomic layer deposition of TiO<sub>2</sub> on mesoporous silica. *J Non-Cryst Solids* 2006, **352**(30): 3280-3284.
- 8. Weng Z, Chen Z-h, Qin X, Zaera F. Sub-monolayer control of the growth of oxide films on mesoporous materials. *J Mater Chem A* 2018, **6**(36): 17548-17558.
- 9. Anderson R, Mountjoy G, Smith ME, Newport RJ. An EXAFS study of silica–titania sol–gels. *J Non-Cryst Solids* 1998, **232-234:** 72-79.
- 10. Mergel D, Buschendorf D, Eggert S, Grammes R, Samset B. Density and refractive index of TiO<sub>2</sub> films prepared by reactive evaporation. *Thin Solid Films* 2000, **371**(1): 218-224.

- 11. Matthias A, Raićevic N, Donfeu Tchana R, Kip D, Deubener J. Density dependence of refractive index of nanoparticle-derived titania films on glass. *Thin Solid Films* 2014, **558**: 86-92.
- 12. Angelomé PC, Andrini L, Calvo ME, Requejo FG, Bilmes SA, Soler-Illia GJAA. Mesoporous Anatase TiO2 Films: Use of Ti K XANES for the Quantification of the Nanocrystalline Character and Substrate Effects in the Photocatalysis Behavior. *J Phys Chem C* 2007, **111**(29): 10886-10893.
- 13. Blanco E, González-Leal JM, Ramírez-del Solar M. Photocatalytic TiO<sub>2</sub> sol–gel thin films: Optical and morphological characterization. *Solar Energy* 2015, **122**: 11-23.
- 14. Song L, Körstgens V, Magerl D, Su B, Fröschl T, Hüsing N, *et al.* Low-Temperature Fabrication of Mesoporous Titania Thin Films. *MRS Advances* 2017, **2**(43): 2315-2325.
- 15. Albert K, Bayer E. Characterization of bonded phases by solid-state NMR spectroscopy. *Journal of Chromatography A* 1991, **544:** 345-370.
- 16. Pallister PJ, Barry ST. Surface chemistry of group 11 atomic layer deposition precursors on silica using solid-state nuclear magnetic resonance spectroscopy. *J Chem Phys* 2017, **146**(5): 052812.
- 17. Weng Z, Yu T, Zaera F. Synthesis of Solid Catalysts with Spatially Resolved Acidic and Basic Molecular Functionalities. *ACS Catal* 2018, **8:** 2870-2879.
- 18. Zhang H, Chen B, Banfield JF, Waychunas GA. Atomic structure of nanometer-sized amorphous TiO<sub>2</sub>. *Phys Rev B* 2008, **78**(21): 214106.
- 19. Sahoo M, Yadav AK, Ghosh S, Jha SN, Bhattacharyya D, Mathews T. Structural studies of spray pyrolysis synthesized oxygen deficient anatase TiO<sub>2</sub> thin films by using X-ray absorption spectroscopy. *Phys Chem Chem Phys* 2019, **21**(11): 6198-6206.
- 20. Chen LX, Rajh T, Wang Z, Thurnauer MC. XAFS Studies of Surface Structures of TiO<sub>2</sub> Nanoparticles and Photocatalytic Reduction of Metal Ions. *J Phys Chem B* 1997, **101**(50): 10688-10697.
- 21. Naicker PK, Cummings PT, Zhang H, Banfield JF. Characterization of Titanium Dioxide Nanoparticles Using Molecular Dynamics Simulations. *J Phys Chem B* 2005, **109**(32): 15243-15249.
- 22. Chen X, Mao SS. Titanium Dioxide Nanomaterials: Synthesis, Properties, Modifications, and Applications. *Chem Rev* 2007, **107**(7): 2891-2959.
- Zhang H, Banfield JF. Structural Characteristics and Mechanical and Thermodynamic Properties of Nanocrystalline TiO2. *Chem Rev* 2014, **114**(19): 9613-9644.

- 24. Lu Z, Liu X, Zhang B, Gan Z, Tang S, Ma L, *et al.* Structure and reactivity of single site Ti catalysts for propylene epoxidation. *J Catal* 2019, **377:** 419-428.
- 25. Cao Y, Chen B, Guerrero-Sánchez J, Lee I, Zhou X, Takeuchi N, *et al.* Controlling Selectivity in Unsaturated Aldehyde Hydrogenation Using Single-Site Alloy Catalysts. *ACS Catal* 2019, **9:** 9150-9157.